ADVANCED MATERIALS

www.advmat.de

Porous Silicon Nanoparticle Delivery of Tandem Peptide Anti-Infectives for the Treatment of *Pseudomonas aeruginosa* Lung Infections

*Ester J. Kwon, Matthew Skalak, Alessandro Bertucci, Gary Braun, Francesco Ricci, Erkki Ruoslahti, Michael J. Sailor, and Sangeeta N. Bhatia**

There is an urgent need for new materials to treat bacterial infections. In order to improve antibacterial delivery, an anti-infective nanomaterial is developed that utilizes two strategies for localization: i) a biodegradable nanoparticle carrier to localize therapeutics within the tissue, and ii) a novel tandem peptide cargo to localize payload to bacterial membranes. First, a library of antibacterial peptides is screened that combines a membrane-localizing peptide with a toxic peptide cargo and discovers a tandem peptide that displays synergy between the two domains and is able to kill *Pseudomonas aeruginosa* at sub-micromolar concentrations. To apply this material to the lung, the tandem peptide is loaded into porous silicon nanoparticles (pSiNPs). Charged peptide payloads are loaded into the pores of the pSiNP at ≈30% mass loading and ≈90% loading efficiency using phosphonate surface chemistry. When delivered to the lungs of mice, this anti-infective nanomaterial exhibits improved safety profiles over free peptides. Moreover, treatment of a lung infection of *P. aeruginosa* results in a large reduction in bacterial numbers and markedly improves survival compared to untreated mice. Collectively, this study presents the selection of a bifunctional peptide-based anti-infective agent and its delivery via biodegradable nanoparticles for application to an animal model of lung infection.

A global threat in the fight against pathogenic bacteria has emerged with the rising incidence of antibiotic resistance combined with the paucity of new antibacterial agents entering the clinic. Two major obstacles facing the development of new antibiotics are poor drug penetration into bacteria and off-target toxicity. Improved delivery has the potential to address these challenges. Here, we engineered nanomaterials for antibacterial activity employing two strategies to improve delivery which have not yet been explored for treatment of lung infections. First, we screened a library of bifunctional peptides that can localize to bacterial membranes and deliver a toxic payload that can specifically kill *Pseudomonas aeruginosa* over off-target host cells. Second, we protected the peptide cargo in biodegradable porous silicon nanoparticles (pSiNPs) to delay and extend the release after lung delivery. Antibiotic delivery via pSiNPs has yet to be established for treatment of lung infections.[1,2] Together, these elements combined to form an anti-infective nanomaterial that we applied to a *P. aeruginosa* lung infection model (**Figure 1**A). We found the anti-infective nanomaterial significantly decreased bacterial numbers and improved survival in a mouse model of lung infection.

In *P. aeruginosa*, two concentric membrane structures studded with efflux pumps surround the degradative periplasmic compartment,[3] creating a formidable barrier for antibacterial agents. We hypothesized that peptides could offer a means to specifically localize to bacteria, either by ligand-mediated binding and/or other physical interaction with membranes. Peptides are

Dr. E. J. Kwon, M. Skalak
Koch Institute for Integrative Cancer Research and Harvard-MIT Division of Health Sciences and Technology
Massachusetts Institute of Technology
Cambridge, MA 02139, USA

Dr. A. Bertucci, Prof. M. J. Sailor
Department of Chemistry and Biochemistry
University of California at San Diego
La Jolla, CA 92093, USA

Dr. A. Bertucci, Prof. F. Ricci
Dipartimento di Scienze e Tecnologie Chimiche
University of Rome
Tor Vergata, Via della Ricerca Scientifica, Rome 00133, Italy

DOI: 10.1002/adma.201701527

Dr. G. Braun, Prof. E. Ruoslahti
Cancer Research Center
Sanford Burnham Prebys Medical Discovery Institute
La Jolla, CA 92037, USA

Prof. S. N. Bhatia
Koch Institute for Integrative Cancer Research, Institute for Medical Engineering and Science
Harvard-MIT Division of Health Sciences and Technology
Electrical Engineering and Computer Science
Massachusetts Institute of Technology
Cambridge, MA 02139, USA
E-mail: sbhatia@mit.edu

Prof. S. N. Bhatia
Howard Hughes Medical Institute
Massachusetts Institute of Technology
Cambridge, MA 02139, USA

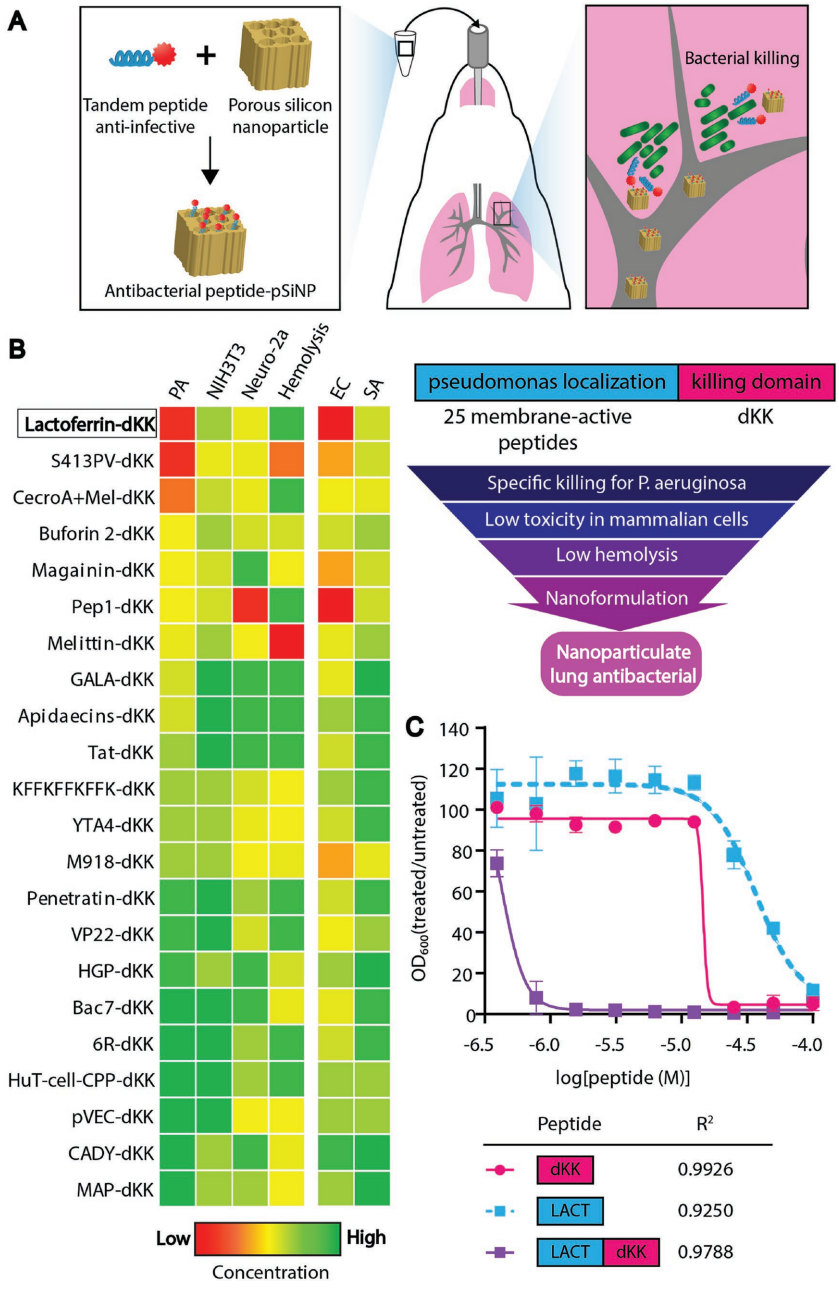

Figure 1. Selection of a pseudomonas-specific anti-infective tandem peptide. A) The overall approach was to design materials composed of an anti-infective peptide cargo loaded in biodegradable porous silicon nanoparticles for delivery to lung infection models. B) Approach used to design and screen tandem peptides for anti-infective activity against *P. aeruginosa*, where candidates were selected based on their capacity to specifically kill bacteria while minimizing toxicity to the host tissue and blood cells. Peptide candidates were first ranked based on the minimum inhibitory concentration (MIC) required to inhibit *P. aeruginosa* (PA) growth (left column, MIC values ranked from low to high for most efficacious peptides on top). Peptide concentrations were tested in the concentration range 0–5 × 10^{-6} M. The next two columns to the right show the level of exposure that leads to 50% lethality (LD50) in NIH3T3 normal fibroblasts and Neuro-2a mouse neuroblastoma cells, respectively. The next column represents the relative concentration required to lyse 10% of red blood cells. Ranked peptides were also cross-validated (last two columns on the right) for their MIC in *Escherichia coli* (EC) and *Staphylococcusaureus* (SA). The top scoring tandem peptide, lactoferrin-dKK, is highlighted in the box. C) LACT-dKK tandem peptide and individual peptide domains (dKK and LACT only) were compared in a MIC assay (average ± SD, $n = 3$) where bacteria were incubated with peptides and the bacterial turbidity was measured at 600 nm at 14 h. Data points were fit with dose response curves. Tandem peptide (purple) shows a greater than 30-fold improvement in MIC over single peptide domains, and Bliss independence analysis indicates that the activity is synergistic. R^2 values are reported for each curve-fit.

promising building blocks because they possess diverse abilities such as binding to specific receptors,[4] stimulating, or blocking signaling cascades, or forming structures that interact with membranes,[5] and there are emerging strategies available that can optimize and stabilize peptides for translation as therapeutics in living systems.[6] In order to enhance bacterial interaction, we designed and tested a library of membrane-interacting peptides fused in tandem with a synthetic bacterial toxin, $_D$[KLAKLAK]$_2$.[7,8] The antibacterial activity of the [KLAKLAK]$_2$ peptide is not dependent on its stereochemistry,[8,9] thus we synthesized it with D-amino acids to limit proteolytic degradation and refer to it as dKK. We reasoned that the dKK bacterial toxin would achieve greater potency if it localized to the bacterial surface—since a toxic payload must first physically encounter the bacteria in order for it to have activity. We focused on the membrane in particular; studies in mutant strains have shown membrane permeability to be a significant barrier to the activity of antibiotics in Gram-negative bacteria.[10] Therefore, we designed our peptide library to encompass membrane-interacting peptides in tandem with the toxic dKK cargo: we chose 25 peptides documented to have membrane-active properties and grafted them N-terminally to dKK (22 of the 25 tandem peptides were soluble in water; Table S1, Supporting Information).

We screened this tandem peptide library using a series of assays to identify agents that mediated specific killing of *P. aeruginosa*, and that also exhibited limited off-target toxicity (Figure 1B). We measured minimal inhibitory concentrations (MIC) in *P. aeruginosa* and cell viability in mammalian cell assays in a peptide concentration range between 0 and 5 × 10^{-6} M. We also evaluated toxicity in NIH3T3 mouse fibroblasts and Neuro-2a neuroblastoma cells. To negatively select against tandem peptides that would cause lysis of red blood cells when administered in animals, we additionally screened peptides in a hemolysis assay. In the range of concentrations we tested, no membrane-active peptide displayed inhibitory activity against bacteria when not in tandem with dKK (Figure S1, Supporting Information), supporting the rationale of the tandem peptide architecture.

We also note that at the concentrations studied, dKK alone had no activity against *P. aeruginosa* (Figure S1, Supporting Information). Since it is advantageous to identify antibacterial agents that possess narrow-spectrum activity, we also assessed antibacterial efficacy against other Gram-negative bacterial species (*Escherichia coli*) and a Gram-positive bacterial species (*Staphylococcus aureus*; Figure 1B). Our best-performing tandem peptide was lactoferrin-dKK (LACT-dKK). Lactoferrin peptide (KCFQWQRNMRKVRGPPVSCIKR) is derived from a protein in the transferrin family that is known to interact with bacterial membranes.[11] Analysis of physicochemical properties of peptides did not predict relative activity for killing *P. aeruginosa* (Table S1, Supporting Information), indicating the need for empirical screening. High-purity LACT-dKK was synthesized and the dose–responses of dKK alone, membrane-active peptide alone, and candidate tandem peptides were tested at concentrations up to 100×10^{-6} M (Figure 1C). LACT-dKK killed bacteria at a sub-micromolar concentration (0.42×10^{-6} M), 128-fold more potent than LACT alone and 32-fold more potent than dKK alone, and was able to associate with *P. aeruginosa* (Figure S2, Supporting Information). As a comparison, the antibiotic colistin was also tested and the MIC was measured to be 0.25 μg mL^{-1} or 0.21×10^{-6} M. When dose-response curves were tested for Bliss independence[12] (GraphPad Prism, GraphPad Software, Inc.), the tandem peptide-mediated killing exceeded the expected additive response of the two single peptide domains, indicating synergy between the two peptide domains in the tandem peptide construct.

To minimize toxicity, we formulated our best performing peptide into nanoparticles to influence peptide biodistribution by increasing local concentrations and mitigating off-target toxicity profiles—a challenge for all peptide-based antibacterial agents in therapy.[13] In cancer therapy, it is well established that packaging chemotherapeutics into nanometer-sized carriers can reduce clinical side effects; for example, cardiotoxicity of doxorubicin is substantially reduced when formulated in Doxil liposomal nanoparticles.[14] As a strategy to improve biodistribution and mitigate toxicity, peptides were loaded in biodegradable pSiNPs, which have been utilized in several applications of drug delivery.[15–18] For example, the flexibility of modifying the physicochemical properties of porous silicon has enabled the delivery of diverse cargoes such as nucleic acids[19] as well the controlled release of hydrophobic cancer therapeutics.[20] Several features of pSiNPs make them amenable to noncovalent peptide loading and release in vivo: i) tunable pore sizes (2–50 nm) that can readily accommodate a range of biomolecule sizes; ii) a suite of surface chemistries available to control physicochemical properties such as charge and hydrophobicity; and iii) a biocompatible degradation pathway whose end products are removed from the body via efficient excretion into the urine.[17,21,22] pSiNPs were prepared as described previously,[23] and displayed a hydrodynamic diameter of 225 ± 10 nm as measured by dynamic light scattering (DLS; $n = 6$, representative plot in Figure S3A, Supporting Information). The porous layer porosity was measured to be 46% ± 1 using spectroscopic liquid infiltration method (SLIM), a nondestructive optical interferometric technique described previously.[24] In order to optimize the loading capacity of the nanoparticle formulation, we investigated a set of different chemical functionalizations to mediate physical interactions with the peptide cargo. The surface of pSiNPs was modified with phosphonates, carboxylates, sulfonates, and amines via silane chemistry and subsequent loading of peptide was achieved by infiltration (**Figure 2**A). Functionalization was confirmed by infrared spectroscopy (Figure 2B; and Figure S3B, Supporting Information). Of the surface chemistries investigated, phosphonate modification yielded the highest (≈30%) loading efficiency (microgram peptide per microgram porous silicon) of peptide (Figure 2C) as measured by quantification of unloaded 5-carboxyfluorescein (5-FAM)-labeled peptide, and was comparable to other charge-based assemblies of pSiNPs.[17,25,26] Phosphonate modified pSiNPs also displayed high encapsulation efficiency (88.0 ± 3.7%, $n = 3$), likely driven by strong electrostatic interactions between the negatively charged phosphonate-modified pores of pSiNP and the positively charged peptide cargo (Figure 2A, inset). Additionally, thermogravimetric analysis of phosphonate pSiNPs yielded a 14.1% weight loss, indicating an average grafting of 140 μg of alkyl-phosphonate chains per mg of pSiNP (Figure S3C, Supporting Information). Zeta potential measurements of oxidized pSiNPs, phosphonate pSiNPs, and peptide-loaded pSiNPs revealed a negative surface potential for all the particle types measured (Figure 2D). Comparing transmission electron microscopy images of unloaded pSiNPs and peptide-loaded pSiNPs showed that the porous structure was maintained in each case (Figure 2E). Total pore volumes and average pore sizes were calculated from nitrogen adsorption–desorption isotherms (Figure 2F) using the Brunauer–Emmett–Teller (BET) method.[27] The total pore volume and average pore size for pSiNPs were 1.33 cm^3 g^{-1} and 14.4 nm and for phosphonate pSiNPs they were 1.17 cm^3 g^{-1} and 13.3 nm, respectively. The reduction in pore volume and size are consistent with oxidation and functionalization of pSiNPs, and the pore size is sufficient to accommodate the ≈4800 molecular weight peptide. Although all particle types displayed a net negative surface charge, the phosphonate modification showed values of zeta potential that were more negative than the oxidized pSiNP starting material, whereas the peptide-loaded phosphonate pSiNPs showed a less negative zeta potential than the oxidized pSiNPs. The negative zeta potential for peptide-loaded phosphonate pSiNPs indicates that the surface negative charge was not completely neutralized by surface-bound peptide (since the peptide itself carries a positive charge), and that at least a portion of the peptides had loaded into the pores. The release of peptide from phosphonate pSiNPs was monitored by incubation in phosphate buffered saline (PBS) and measuring fluorescently labeled peptide released into the supernatant after centrifugation of intact pSiNPs (Figure 2G) and matches with the degradation profile of pSiNPs (Figure S3D, Supporting Information). Peptides formulated into phosphonate pSiNPs were able to mediate killing of *P. aeruginosa* (Figure 2H) while showing minimal toxicity to mammalian cells (**Figure 3**A) and minimal red blood cell lysis (Figure 3B).

To examine the utility of this peptide–pSiNP platform in vivo, we delivered peptide-loaded phosphonate pSiNPs (peptide–pSiNP) in the context of a *P. aeruginosa* lung infections. We first tested the histological response of the nanomaterials after direct administration to the lungs of healthy mice. Sample solutions (PBS, unloaded pSiNPs, free peptide,

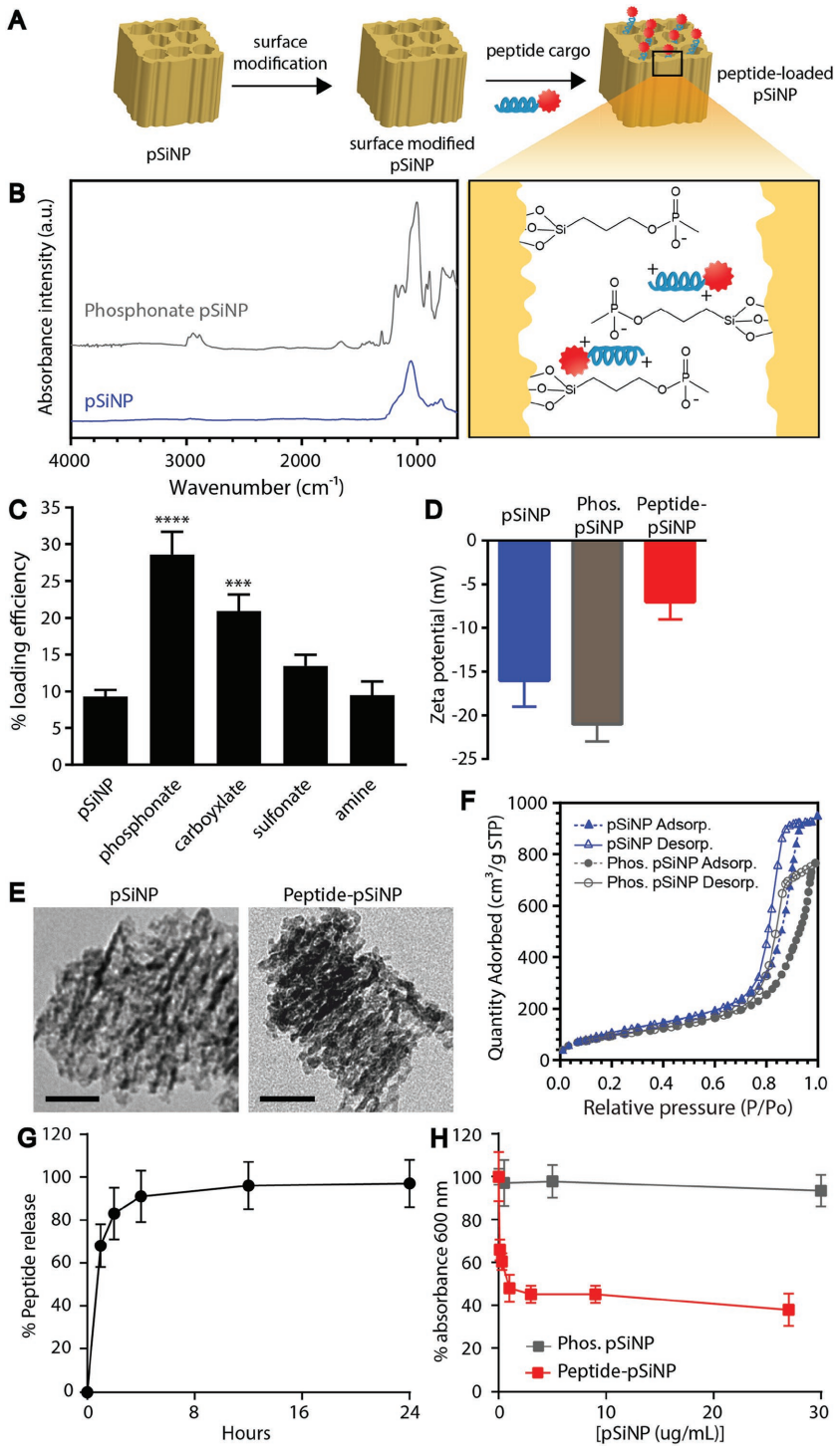

Figure 2. Tandem peptide infiltrated in porous silicon nanoparticles maintain anti-infective properties. A) Schematic outlining the approach to loading tandem peptide cargo into surface modified porous silicon nanoparticles (pSiNPs). Inset depicts proposed electrostatic interaction of phosphonate pSiNP with cationic tandem peptides. B) Fourier transform infrared (FTIR) spectrum of pSiNP and phosphonate pSiNP. Si–O–Si modes can be observed from 790–1100 cm^{-1} in the pSiNP spectrum. Phosphonate pSiNP spectrum shows appearance of aliphatic C–H (2800–3000 cm^{-1}) and P=O (1300 cm^{-1}), and the deformation of –OH from –POOH (1650 cm^{-1}). IR spectra of carboxylate, sulfonate, and amine pSiNP can be found in Figure S3B (Supporting Information). C) Effect of modified surface chemistry on peptide loading efficiency (mass percentage, $n = 3$, average +SD, ****$p < 0.0001$, ***$p < 0.001$ analysis of variance (ANOVA)). D) Zeta potential measurements of pSiNPs, phosphonate modified pSiNPs, and peptide–pSiNPs (average –SD, $n = 4$). E) Transmission electron microscopy images of unmodified pSiNP and peptide–pSiNPs (scale bar = 50 nm). F) Cryogenic nitrogen adsorption–desorption isotherms of pSiNPs and phosphonate pSiNPs. G) Release of peptide from pSiNPs into phosphate buffered saline (PBS) was determined by measuring fluorescence signal of peptide in the supernatant over the course of 24 h (average ±SD, $n = 3$). H) Killing activity of peptide–pSiNPs against *P. aeruginosa*, based on bacterial turbidity measurements (average ±SD, $n = 3$).

or peptide–pSiNP) were instilled into the lung via a catheter inserted into the trachea. Mice that received free peptide displayed slowed, labored breathing compared to PBS-treated mice between 4 and 8 h after dosing, whereas no adverse respiration was observed with mice administered peptide–pSiNPs. To correlate these observations with any changes in tissue pathology and circulating cytokine levels, organs and blood were harvested at 4 or 24 h after dosing. Hemotoxylin and eosin staining of lung sections were assessed by a pathologist blinded to treatment conditions. Lungs from untreated mice and mice administered either peptide-loaded or empty pSiNPs displayed generally normal morphology, and peptide–pSiNP-administered mice presented with mild bronchial epithelial damage (Figure 3C; top row). The normal histology observed in mice after pSiNP administration corroborates previous work that demonstrated that pSiNPs administered at a dosage of 400 µg per mouse showed no evidence of toxicity after 4 weeks.[22] By contrast, evidence of damage in the lungs at 4 h after administration of free peptide was substantial as assessed by the pathologist: sloughing of the bronchial epithelium, bronchitis, and interstitial pneumonitis were all observed (Figure 3C; bottom row). The toxicity of the tandem peptide cargo may be due to its cationic nature; toxicity of cationic materials has been observed previously.[28] However, evidence of toxicity appeared to subside by 24 h and was not observed in any other organs (Figure S4, Supporting Information), indicating a local and transient response. To investigate the molecular pathways involved at the time point during which we observed histological changes, we assayed serum collected from mice at 4 h for the presence of a panel of cytokines and revealed upregulation of cytokines documented as part of the acute response to antimicrobial peptides,[29]

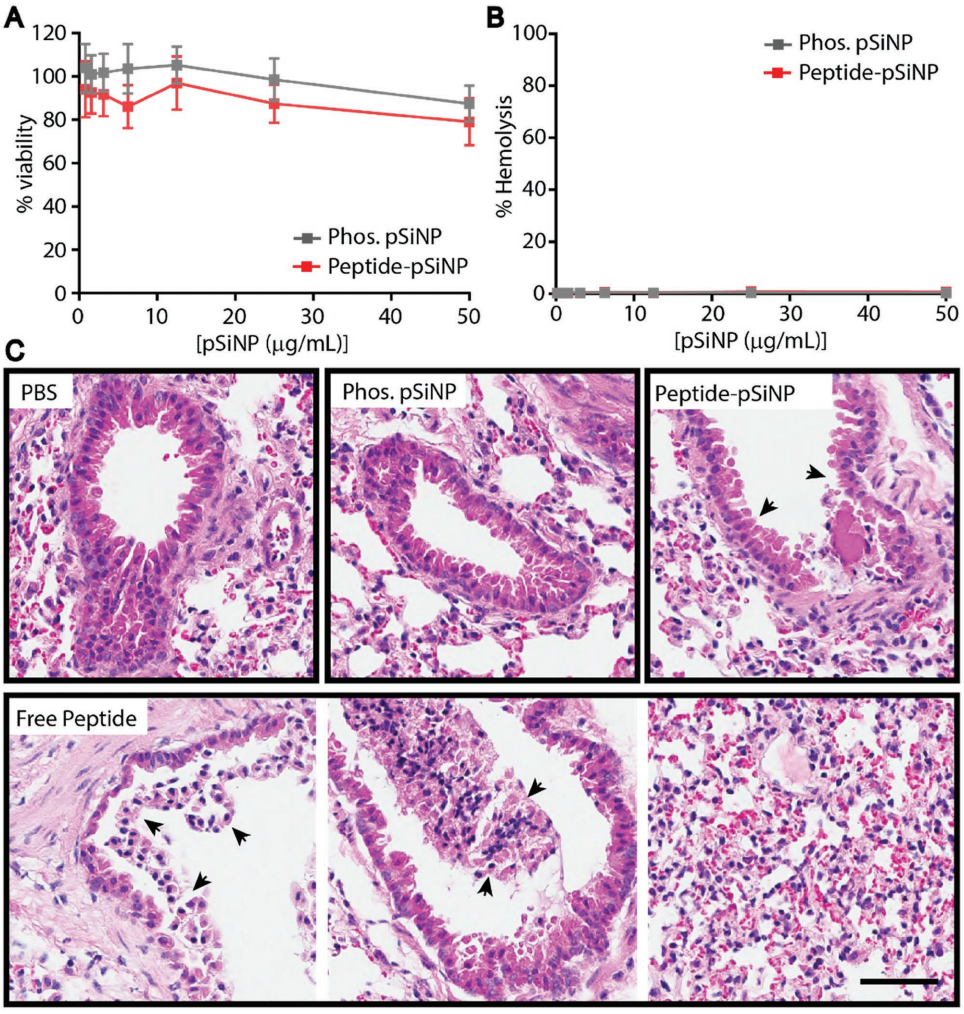

Figure 3. pSiNP formulation of peptides improve toxicity profile. Evaluation of peptide–pSiNPs for A) NIH-3T3 mammalian cell toxicity at 48 h, and B) hemolysis of red blood cells. Plots (A) and (B) are plotted as means ± SD ($n = 3$). C) Histology of lungs of uninfected mice 4 h after lung delivery of (top) PBS, phosphonate pSiNP, peptide–pSiNPs, or (bottom) free peptide. Histological features were identified by a pathologist blinded to treatment conditions. Arrowheads indicate signs of mild lung epithelial damage (peptide–pSiNPs), epithelial sloughing, and bronchitis (free peptide; bottom, left to right). Free-peptide-treated mice also had signs of interstitial pneumonitis (bottom, far right panel). Phenotypes detected in the free peptide administered lungs were not observed in the other groups of mice. Scale bar represents 50 μm ($n = 3$ per treatment, representative image shown).

in particular an increase in cytokine IL-6 in mice administered free peptide compared to the other treatment groups (Figure S5, Supporting Information). These results are consistent with the histopathological analysis. Taken together, the mouse behavior, histopathology, and cytokine data indicated that free peptide generated too severe of an acute adverse response be suitable as a therapeutic, and present a strong motivation to sequester the toxic peptide antibacterial agents during administration. The free peptide data underscored the need for a suitable biodegradable carrier for sustained release in the lungs, in order to reduce the immediate inflammatory response generated by a large bolus insult. We therefore performed the subsequent functional studies using only peptide formulated into pSiNPs.

In order to assess the therapeutic impact of peptide–pSiNP administration, we applied our peptide nanomaterial to a mouse model of *P. aeruginosa* lung infection. PA01 was instilled into the lungs via a catheter and infection levels were determined by titering the number of colony forming units (CFU) harvested from lung tissue. We first characterized the localization of peptide–pSiNP in the context of *P. aeruginosa* pneumonia. We examined the distribution of fluorescently labeled peptide payload delivered 2 and 4 h after the mice were inoculated with bacteria via lung instillation. Organs were retrieved and assessed for payload fluorescence 4 h after the last administration. Signal was detected in the lungs, whereas no detectable off-target organ accumulation was observed, as expected from a direct lung administration route (**Figure 4**A; and Figure S6A, Supporting Information). Staining and imaging of cross-sections through the lung reveal widespread distribution of both peptide and *P. aeruginosa* throughout the tissue, and a representative image is shown in Figure 4B. Cellular-level examination of untreated and peptide–pSiNP-treated lungs reveal some evidence of payload internalization into F4/80$^+$ resident

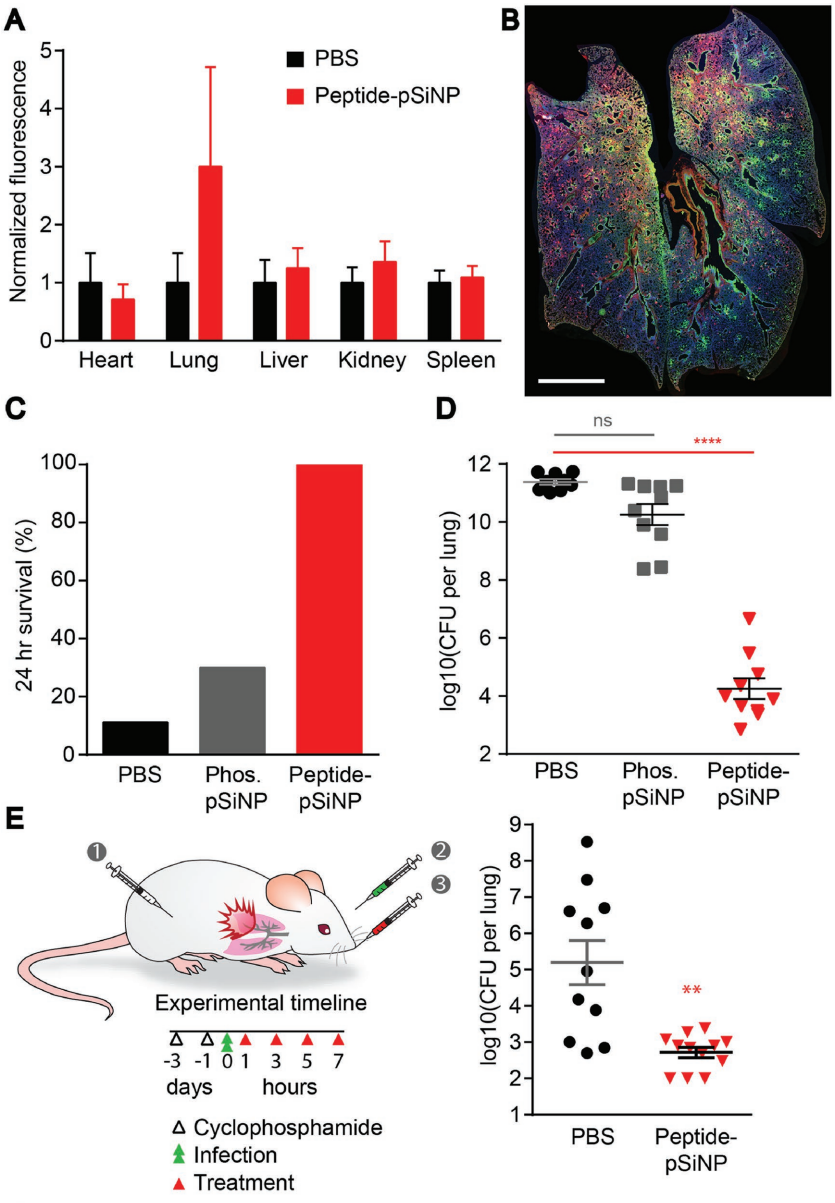

F

Strain	Ciprofloxacin	Imipenem	Ceftazidime	Piperacillin	Levofloxacin	Peptide (MIC)
PAO1	S	S	S	S	S	S
Clinical Isolate 1	R	R	R	R	R	S
Clinical Isolate 2	S	R	S	S	S	S
Clinical Isolate 3	S	S	S	S	S	S
Clinical Isolate 4	S	R	S	S	S	S
Clinical Isolate 5	S	S	S	S	S	S

Figure 4. Peptide–pSiNP efficacy in an animal model of *P. aeruginosa* lung infection. A) Quantification of bulk peptide signal normalized to mice administered PBS visualized by imaging the fluorescent tag on peptides using IVIS imaging ($n = 3$, mean +SEM. IVIS image available in Figure S5, Supporting Information). Mice were dosed with material 2 and 4 h postinfection and organs harvested 8 h postinfection. B) Representative whole-lung cross-section of peptide (green) and *P. aeruginosa* (PA) (red) distribution in the lung (scale bar = 2 mm). Tissue was imaged on a slide scanner and lung tissue was cropped and put on a black background to remove surrounding autofluorescence of the hydrophobic barrier pen used in staining. Agents were first evaluated after cotreatments of bacteria and anti-infective agents in a high titer infection model that results in ≈10% 24 h survival. C) Percentage of mice that survived for at least 24 h after coadministration of intratracheal *P. aeruginosa* and PBS, pSiNP, or peptide–pSiNP, and D) bacterial CFU recovered from lungs at this time point ($n = 9$–10, average ±SEM, ****$p < 0.0001$ ANOVA. Two independent trials). E) Left, schematic of experimental design, modified for physiologic infection timescales of infection with *P. aeruginosa* to allow for intervention with 100% survival at 24 h. Cyclophosphamide was administered intraperitoneally to deplete neutrophils 3 d prior to infection. Bacterial CFU titered from lungs of mice 24 h post-treatment with peptide–pSiNP, compared to PBS control ($n = 11$–12 mice, average ± SEM, **$p < 0.01$ two-tailed Mann–Whitney. Two independent trials.) F) PA01 and five clinical isolates with reported antibiotic susceptibility (S) or resistance (R) were dosed with peptide to determine the MIC (right column) in each case. All isolates examined exhibited susceptibility to peptide killing (measured MIC for all clinical isolates was between 2 and 4 times the MIC of the PA01 strain).

interstitial and alveolar macrophages, but not into infiltrating CD11b$^+$ monocytes recruited to the infected areas (Figure S6B, Supporting Information).

Improvement of survival and bacterial titers after peptide–pSiNP administration were quantified in the *P. aeruginosa* lung infection model. At 2×10^5 CFU per mouse, development of lung infection with *P. aeruginosa* was aggressive, with only 10–20% 24 h survival without therapeutic intervention. We first tested the potential therapeutic efficacy of peptide–pSiNP materials when coadministered with the bacteria at this high titer inoculum. For this study, mice were given two doses of peptide–pSiNPs at 30 µg of pSiNPs and 1.5 nmoles peptide, or the equivalent amount of empty pSiNP carrier. The first dose was administered at the time of infection and the second was administered 2 h postinfection. The mice were observed and their lungs harvested at the survival endpoint, or at 24 h postinfection. The peptide–pSiNP formulations greatly improved the survival to 24 h. A lower than 20% survival was observed with vehicle treatment, and this increased to 100% survival with the peptide–pSiNP formulation (Figure 4C). To confirm that the improvement in survival was due to decreased lung titers of *P. aeruginosa*, we excised lungs and titered the number of CFU

in the organ. Treatment of mice with empty pSiNPs appeared to cause a decrease in number of bacteria in the lung, but the difference to control treatment was not statistically significant. We observed a dramatic decrease in bacterial count when were administered peptide–pSiNPs, with lung titers 4–6 $\log_{10}$ lower than when no therapeutic intervention was administered (Figure 4D).

Based on the encouraging coadministration findings, we determined if the construct could perform as a more clinically relevant anti-infective, by administering the peptide–pSiNP material 1 h after bacterial instillation. Mice were infected with 1×10^3 CFU *P. aeruginosa*/mouse to establish an infection that resulted in near 100% 24 h survival. This model allowed for reliable quantification of infection by assaying the lungs of the animals for bacteria. The mice were treated at 1, 3, 5, and 7 h after infection with 2 nmoles of peptide/40 μg of pSiNP per dose (equivalent to 10 μg of peptide). The lungs were harvested at 24 h and titered for bacteria. Untreated mice had titers that ranged from $\log_{10}$ 2–9 with an average $\log_{10}$ value of 5.2 CFU per lung, whereas mice treated with peptide–pSiNP had an average $\log_{10}$ value of 2.7 CFU per lung (Figure 4E). Total dosage of anti-infective peptide was 0.7 mg kg^{-1} per mouse for cotreatment and 1.9 mg kg^{-1} for post-treatment, on par with the 1.5–2.5 mg kg^{-1} dosing used clinically for colistin.[30] The frequency of dosing was also chosen to reflect dosage in human patients, where aerosolized colistin was administered every 6 h in patients with lung infections.[31] Colistin, a peptide-based antibacterial considered a drug of last resort due to its toxicity profile, has limited efficacy in the context of pneumonia,[32] supporting the benefit of developing additional agents to combat infections. We believe with further fine-tuning, such as sequence optimization, increased solubility, and chemical stabilization, it is possible to engineer even more potent agents around the peptide identified and used in the present studies.

Finally, to determine whether the tandem peptide anti-infective was extensible to other strains of *P. aeruginosa* beyond the laboratory strain PA01, we tested peptide in clinical isolates taken from human patient lungs (Figure 4F). Of the five clinical isolates tested, three of the strains are resistant to first-line antibiotics as reported previously.[33] We found that all strains we evaluated were susceptible to the tandem peptide construct, and displayed MIC values between two- and four-fold larger than the MIC for the PA01 strain.

The goal of this study was to engineer a highly effective antibacterial agent using a peptide-based toxin enclosed in a biodegradable nanoparticle delivery vehicle. We screened a library of tandem peptide anti-infectives that contained a bacterial membrane-interaction domain grafted to a domain with bactericidal activity. We discovered a tandem peptide anti-infective with highly synergistic activity between its two domains; efficacy of the tandem peptide was >30-fold higher than either of its individual components. The MIC measured for the tandem peptide antibacterial was sub-micromolar, comparable to the MIC measured for the antibiotic colistin. We formulated the best performing peptide into a biodegradable pSiNP nanoparticle, and achieved significant decreases in bacteria titers after delivery to the lung in a mouse model of lung infection. Clinical isolates from human lung infections were susceptible to peptide killing, supporting that this agent could be applied to other strains of *P. aeruginosa*. Modifications of this material for future application to human lungs would include dry formulations for aerosol delivery and micrometer scale particle sizes for optimal deposition in the architecture of human lungs,[34] design criteria that could both be satisfied by the pSiNP platform. Beyond reducing toxicity, nanoparticles can package combinations of drugs such as small molecules[35] without the need for covalent modification, be modified to target specific tissues and cell types,[36] and be encoded with "smart" properties.[37]

Experimental Section

Peptide Synthesis: The peptide library in Table S1 (Supporting Information) was synthesized for initial screening with FAM-conjugated lysine at the C-terminal end of the membrane-interactive peptide and with or without D[KLAKLAK]2 on the C-terminus using standard Fmoc chemistry by the Koch Institute Swanston Biotechnology Center. All peptides were synthesized with N-terminal myristic acid and C-terminal amine. They were resynthesized to 80% purity in small lots for follow-up in vitro studies. For the animal studies, larger quantities of the peptides were synthesized by CPC Scientific to 90% purity.

Porous Silicon Nanoparticle Preparation: The particles were prepared as described previously.[23] Briefly, highly boron-doped p^{++}-type crystalline silicon wafers, polished on the (100) face, were electrochemically etched in an electrolyte consisting of 3:1 (v:v) 48% aqueous hydrofluoric acid (HF):ethanol under current control (CAUTION: HF is highly corrosive to the eyes and skin and proper precautions should be followed when handling). The etching waveform consisted of a current-density–time profile consisting of two current levels (50 mA cm^{-2} for 1.8 s; 400 mA cm^{-2} for 0.36 s), repeated for 150 cycles The resulting film was removed from the silicon substrate by application of a current density pulse of 3.7 mA cm^{-2} for 250 s in 1:29 (v:v) 48% aqueous HF:ethanol and fragmented by ultrasonication overnight. The resulting pSiNPs were dispersed in an aqueous solution of sodium tetraborate to grow a thin layer of silicon oxide on the particle surface.

Surface Functionalization of pSiNPs: Amine groups were introduced by stirring the pSiNPs overnight in an ethanol solution 12×10^{-3} M in 3-aminopropyl-dimethyl-ethoxy silane containing a catalytic amount of triethyl amine (TEA). Carboxylate modification was achieved by overnight reaction of the amine-modified pSiNPs (3 mg) with succinic anhydride (10 mg) in 3 mL of dimethylformamide. Phosphonate modification was achieved by reacting pSiNPs in ethanol with 11.2×10^{-3} M tetraethyl orthosilicate and a catalytic amount of TEA at room temperature for 1 h. Subsequently, 3-(trihydroxysilyl)propyl methylphosphonate was added to a final concentration of 26.3×10^{-3} M and further reacted overnight. Sulfonate modification was carried out following the same procedure as for the phosphonate modification but using 3-(trihydroxysilyl)-1-propane sulfonic acid as the silanating reagent.

Characterization of pSiNPs: The hydrodynamic size and zeta potential of the particles were measured by DLS (Zetasizer ZS90, Malvern Instruments). Size measurements were carried out with particles dispersed in water, whereas the zeta potential analysis was performed in PBS, pH = 7.4. Transmission electron microscopy (TEM) images were acquired with a JEOL-1200 EX II instrument. Attenuated total reflection Fourier transform infrared (FTIR) spectroscopy was collected on a Thermo Scientific Nicolet 6700 instrument. Porous layer porosity was measured using the SLIM, a nondestructive optical interferometric technique described previously.[24] Adsorption–desorption isotherms were performed on dry particles at 77 K on a Micromeritics ASAP 2020 instrument. Total pore volume and average pore sizes were calculated from the adsorption–desorption isotherms using the BET method.

Loading of Peptide in Surface-Modified pSiNPs: Peptide was loaded into phosphonate-pSiNPs by incubating 33% (w:w) peptide:phosphonate

pSiNP for 2 h at room temperature in water at a final peptide concentration of 1 mg mL^{-1}. Peptide–pSiNPs were purified by 3 rounds of centrifugation and resuspension in deionized water. Percent peptide loading was quantified by measuring absorbance of the FAM-labeled peptides recovered in the supernatant after the first centrifugation, as compared to a known calibration curve.

Particle Degradation and Peptide Release Measurements: Particle degradation was measured in PBS, pH 7.4 by monitoring the absorbance intensity at 405 nm over time, as described previously.[38] Peptide-loaded pSiNPs (0.3 mg, $n = 3$) were dispersed in 1 mL of PBS, pH 7.4 at room temperature with mild shaking. The supernatant containing released FAM-labeled peptides was collected at the indicated time points and analyzed by optical absorbance spectroscopy ($\lambda = 495$ nm). Concentrations of the released peptides were determined using a calibration curve obtained with standard solutions of the same peptide in PBS.

Bacterial Preparation: P. aeruginosa PA01 was a generous gift from the Ribbeck Lab at the Massachusetts Institute of Technology. Clinical isolates were a generous gift from the Hung Lab at the Massachusetts General Hospital. For each experiment, bacteria were started from a frozen glycerol stock and cultured overnight. A 1:100 dilution from the overnight culture was grown at 37 °C with shaking to an OD_{600} between 0.2 and 0.6. The number of CFU per mL was determined by titering cultures with known absorbance values.

Overnight Culture Growth Assay: P. aeruginosa strains were diluted in LB media to a final concentration of 2×10^6 CFU mL. For screening, peptides or colistin were tested in triplicates of a series of 8 twofold dilutions starting from 5×10^{-6} M. After 16 h of incubation, bacterial turbidity was examined or the absorbance at 600 nm was measured to determine the MIC.

Hemolysis Assay: Red blood cells were collected from mouse blood harvested in 5×10^{-3} M ethylenediaminetetraacetic acid (EDTA) and stored on ice. Red blood cells were washed in 150×10^{-3} M NaCl and harvested by centrifugation. Red blood cells and peptide were incubated together for 1 h at 37 °C. For screening, peptides were tested in triplicates of a series of 8 twofold dilutions starting from 5×10^{-6} M. Unlysed red blood cells were removed by centrifugation, and released hemoglobin was quantified by measuring absorbance at 541 nm. Percent hemolysis was determined by normalizing to red blood cells incubated with 0.1% Triton-X 100.

Cell Culture: NIH-3T3 and Neuro-2a cells were purchased from the American Type Culture Collection and maintained in Dulbecco's modified Eagle medium and Eagle's minimum essential medium, respectively, supplemented with 10% FBS penicillin–streptomycin.

Mammalian Cell Toxicity Assay: NIH-3T3 or Neuro-2a cells were plated at 2000 cells per well in at 96-well plate 24 h before treatment with peptides at the indicated concentrations for 4 h. Cell viability was measured with the Aqueous One Cell Proliferation Assay (Promega) 48 h after treatment. For screening, peptides were tested in triplicates of a series of 8 twofold dilutions starting from 5×10^{-6} M.

Mouse Tracheal Infection: All animal protocols were carried out in accordance with the MIT IACUC, protocol number 0516-032-19, including the collection of red blood cells for the hemolysis assay described above. 6–8-week-old CD-1 mice were obtained from Charles River. Neutropenia was introduced by injecting cyclophosphamide at 150 mg kg^{-1} 4 d and 100 mg kg^{-1} 1 d preinfection. For the cotreatment study, mice were anesthetized by isoflurane and infected with 2×10^5 CFU in 50 µL by tracheal instillation via a 22G catheter (EXCEL International). Mice received two doses of 1.5 nmole peptide in free form or peptide–pSiNP (≈30 µg of pSiNP) in 50 µL of PBS via tracheal instillation during initial infection and 2 h postinfection. Mice were monitored for 24 h postinfection and lung tissue was collected for homogenization when mice reached euthanasia criteria or at 24 h. For the postinfection treatment study, mice received 1×10^3 CFU and were then treated with four sequential doses of 2 nmole peptide by tracheal instillation. The four doses were administered at 1, 3, 5, and 7 h postinfection. CFUs of PA01 per lung were calculated by plating dilutions of lung homogenates on agar plates and counting colonies. All therapeutic studies were repeated in at least two independent trials.

Animal Toxicity Studies: For toxicity studies, organs were collected 4 or 24 h after the first dose of treatment and organs were drop-fixed in 10% formalin. Organs were embedded in paraffin, cut into 6 µm sections, and stained with hematoxylin and eosin using standard protocols. Signs of tissue damage was assessed by a pathologist blinded to treatment conditions. For cytokine analysis, blood was collected 4 h after first dose of treatment in 5×10^{-3} M EDTA-PBS and red blood cells were cleared by centrifugation. Serum was stored at −80 °C until analysis. Serum was analyzed by Mouse Cytokine Antibody Array, Panel A (R&D Biosystems). Full map of cytokines can be found on the product data sheet. Two mice were used for each time point and condition. Representative images and blots were used for figures.

Distribution Studies: To study the bulk biodistribution of particles in the lung and how they interact with cell types in the lung, particles (1.5 nmole peptide dose) were delivered 2 and 4 h postinfection (2×10^5 CFU per mouse) and animals were sacrificed and organs harvested 8 h after infection. After IVIS imaging of organs, lungs were drop-fixed in 10% formalin overnight, washed with PBS and embedded in paraffin for sectioning.

Histology: Lung sections were blocked in 2% bovine serum albumin, 5% goat serum in PBS and stained for antibodies against pseudomonas (Abcam, 1:500) and fluorescein (Invitrogen, 1:200). Appropriately labeled secondary antibodies were used to detect primary antibodies. Lung scans were acquired on a Perkin Elmer Pannoramic250 and high-magnification images were taken on a Nikon Ti Eclipse microscope.

Statistical Analysis: Statistical tests were done in GraphPad Prism 6 (GraphPad Software, Inc.). Bliss independent testing for synergy was done by simulating a dose–response curve for an additive effect between individual peptides and assessing curve shifting beyond the expected response.

Supporting Information

Supporting Information is available from the Wiley Online Library or from the author.

Acknowledgements

The authors thank the Koch Institute Swanson Biotechnology Center for technical support, specifically Kathleen Cormier and Dr. Roderick T. Bronson in the Hope Babette Tang Histology Facility, and Eliza Vasile of the Microscopy Facility. The authors thank Dr. Heather Fleming (MIT) for critical reading and editing of the manuscript. This study was supported in part by a Koch Institute Support Grant No. P30-CA14051 from the National Cancer Institute (Swanson Biotechnology Center) and a Core Center Grant No. P30-ES002109 from the National Institute of Environmental Health Sciences. This work was also supported in part by the Defense Advanced Research Projects Agency under Cooperative Agreement No. HR0011-13-2-0017. The content of the information within this document does not necessarily reflect the position or the policy of the Government. E.J.K. acknowledges support from the Ruth L. Kirschstein National Research Service Award (No. 1F32CA177094-01). A.B. and F.R. acknowledge support from the Int. Research Staff Exchange Scheme (IRSES) under the EU Marie Curie FP7 program. S.N.B. is a Howard Hughes Medical Institute investigator.

Conflict of Interest

The authors declare no conflict of interest.

Keywords

bacteria, lung infections, nanoparticles, peptides

Received: March 17, 2017
Revised: May 25, 2017
Published online:

[1] C. Sole-Lleonart, J. J. Rouby, S. Blot, G. Poulakou, J. Chastre, L. B. Palmer, M. Bassetti, C. E. Luyt, J. M. Pereira, J. Riera, T. Felton, J. Dhanani, T. Welte, J. M. Garcia-Alamino, J. A. Roberts, J. Rello, *Anesthesiology* **2017**, *126*, 890.
[2] E. Wenzler, D. R. Fraidenburg, T. Scardina, L. H. Danziger, *Clin. Microbiol. Rev.* **2016**, *29*, 581.
[3] T. J. Silhavy, D. Kahne, S. Walker, *Cold Spring Harbor Perspect. Biol.* **2010**, *2*, a000414.
[4] E. Ruoslahti, S. N. Bhatia, M. J. Sailor, *J. Cell Biol.* **2010**, *188*, 759.
[5] H. Sato, J. B. Feix, *Biochim. Biophys. Acta* **2006**, *1758*, 1245.
[6] K. Fosgerau, T. Hoffmann, *Drug Discovery Today* **2015**, *20*, 122.
[7] M. M. Javadpour, M. M. Juban, W. C. Lo, S. M. Bishop, J. B. Alberty, S. M. Cowell, C. L. Becker, M. L. McLaughlin, *J. Med. Chem.* **1996**, *39*, 3107.
[8] D. M. McGrath, E. M. Barbu, W. H. Driessen, T. M. Lasco, J. J. Tarrand, P. C. Okhuysen, D. P. Kontoyiannis, R. L. Sidman, R. Pasqualini, W. Arap, *Proc. Natl. Acad. Sci. USA* **2013**, *110*, 3477.
[9] H. M. Ellerby, W. Arap, L. M. Ellerby, R. Kain, R. Andrusiak, G. D. Rio, S. Krajewski, C. R. Lombardo, R. Rao, E. Ruoslahti, D. E. Bredesen, R. Pasqualini, *Nat. Med.* **1999**, *5*, 1032.
[10] B. L. Angus, A. M. Carey, D. A. Caron, A. M. Kropinski, R. E. Hancock, *Antimicrob. Agents Chemother.* **1982**, *21*, 299.
[11] K. Yamauchi, M. Tomita, T. J. Giehl, R. T. Ellison, *Infect. Immun.* **1993**, *61*, 719.
[12] W. R. Greco, G. Bravo, J. C. Parsons, *Pharmacol. Rev.* **1995**, *47*, 331.
[13] R. Eckert, *Future Microbiol.* **2011**, *6*, 635.
[14] M. E. O'Brien, N. Wigler, M. Inbar, R. Rosso, E. Grischke, A. Santoro, R. Catane, D. G. Kieback, P. Tomczak, S. P. Ackland, F. Orlandi, L. Mellars, L. Alland, C. Tendler, C. B. C. S. Group, *Ann. Oncol.* **2004**, *15*, 440.
[15] T. Tanaka, L. S. Mangala, P. E. Vivas-Mejia, R. Nieves-Alicea, A. P. Mann, E. Mora, H. D. Han, M. M. Shahzad, X. Liu, R. Bhavane, J. Gu, J. R. Fakhoury, C. Chiappini, C. Lu, K. Matsuo, B. Godin, R. L. Stone, A. M. Nick, G. Lopez-Berestein, A. K. Sood, M. Ferrari, *Cancer Res.* **2010**, *70*, 3687.
[16] C. T. Turner, M. H. Kafshgari, E. Melville, B. Delalat, F. Harding, E. Makila, J. J. Salonen, A. J. Cowin, N. H. Voelcker, *ACS Biomater. Sci. Eng.* **2016**, *2*, 2339.
[17] E. J. Anglin, L. Cheng, W. R. Freeman, M. J. Sailor, *Adv. Drug Delivery Rev.* **2008**, *60*, 1266.
[18] E. Tasciotti, X. W. Liu, R. Bhavane, K. Plant, A. D. Leonard, B. K. Price, M. M. C. Cheng, P. Decuzzi, J. M. Tour, F. Robertson, M. Ferrari, *Nat. Nanotechnol.* **2008**, *3*, 151.
[19] J. L. Shen, R. Xu, J. H. Mai, H. C. Kim, X. J. Guo, G. T. Qin, Y. Yang, J. Wolfram, C. F. Mu, X. J. Xia, J. H. Gu, X. W. Liu, Z. W. Mao, M. Ferrari, H. F. Shen, *ACS Nano* **2013**, *7*, 9867.
[20] D. F. Liu, L. M. Bimbo, E. Makila, F. Villanova, M. Kaasalainen, B. Herranz-Blanco, C. M. Caramella, V. P. Lehto, J. Salonen, K. H. Herzig, J. Hirvonen, H. A. Santos, *J. Controlled Release* **2013**, *170*, 268.
[21] J. Siefker, P. Karande, M. O. Coppens, *Expert Opin. Drug Delivery* **2014**, *11*, 1781.
[22] J. H. Park, L. Gu, G. von Maltzahn, E. Ruoslahti, S. N. Bhatia, M. J. Sailor, *Nat. Mater.* **2009**, *8*, 331.
[23] Z. T. Qin, J. Joo, L. Gu, M. J. Sailor, *Part. Part. Syst. Charact.* **2014**, *31*, 252.
[24] E. Segal, L. A. Perelman, F. Cunin, F. Di Renzo, J. M. Devoisselle, Y. Y. Li, M. J. Sailor, *Adv. Funct. Mater.* **2007**, *17*, 1153.
[25] M. Kaasalainen, J. Rytkonen, E. Makila, A. Narvanen, J. Salonen, *Langmuir* **2015**, *31*, 1722.
[26] R. R. Julian, J. L. Beauchamp, *J. Am. Soc. Mass Spectrom.* **2004**, *15*, 616.
[27] S. Brunauer, P. H. Emmett, E. Teller, *J. Am. Chem. Soc.* **1938**, *60*, 309.
[28] H. Lv, S. Zhang, B. Wang, S. Cui, J. Yan, *J. Controlled Release* **2006**, *114*, 100.
[29] S. M. Alalwani, J. Sierigk, C. Herr, O. Pinkenburg, R. Gallo, C. Vogelmeier, R. Bals, *Eur. J. Immunol.* **2010**, *40*, 1118.
[30] A. P. Zavascki, L. Z. Goldani, J. Li, R. L. Nation, *J. Antimicrob. Chemother.* **2007**, *60*, 1206.
[31] M. E. Sobieszczyk, E. Y. Furuya, C. M. Hay, P. Pancholi, P. Della-Latta, S. M. Hammer, C. J. Kubin, *J. Antimicrob. Chemother.* **2004**, *54*, 566.
[32] A. S. Levin, A. A. Barone, J. Penco, M. V. Santos, I. S. Marinho, E. A. Arruda, E. I. Manrique, S. F. Costa, *Clin. Infect. Dis.* **1999**, *28*, 1008.
[33] N. D. Pecora, N. Li, M. Allard, C. Li, E. Albano, M. Delaney, A. Dubois, A. B. Onderdonk, L. Bry, *MBio* **2015**, *6*, e01030.
[34] J. H. Brown, K. M. Cook, F. G. Ney, T. Hatch, *Am. J. Public Health Nations Health* **1950**, *40*, 450.
[35] J. Lu, M. Liong, J. I. Zink, F. Tamanoi, *Small* **2007**, *3*, 1341.
[36] L. Brannon-Peppas, J. O. Blanchette, *Adv. Drug Delivery Rev.* **2004**, *56*, 1649.
[37] E. J. Kwon, J. H. Lo, S. N. Bhatia, *Proc. Natl. Acad. Sci. USA* **2015**, *112*, 14460.
[38] J. Kang, J. Joo, E. J. Kwon, M. Skalak, S. Hussain, Z. G. She, E. Ruoslahti, S. N. Bhatia, M. J. Sailor, *Adv. Mater.* **2016**, *28*, 7962.